



# Optimal electrode placements for localizing premature ventricular contractions using a single dipole cardiac source model

Beata Ondrusova <sup>a</sup>, Peter Tino <sup>b</sup>, Jana Svehlikova <sup>a,\*</sup>

<sup>a</sup> Institute of Measurement Science, Slovak Academy of Sciences, Bratislava, Slovakia

<sup>b</sup> School of Computer Science, University of Birmingham, Birmingham, United Kingdom

## ARTICLE INFO

### Keywords:

Inverse problem of electrocardiography  
ECGI  
Body surface potential mapping  
Optimal electrode placement  
Premature ventricular contractions  
Greedy algorithm

## ABSTRACT

**Introduction:** The inverse problem of electrocardiography describes non-invasively the electrical activity of the heart using potential recordings from tens to hundreds of torso electrodes. Regrettably, the use of numerous electrodes poses a challenge to its integration into routine clinical practice.

**Methods:** Optimal electrode placements, ranging from 8 to 112 electrodes, were derived from the singular values of the transfer matrices computed for all feasible positions of a single dipole cardiac source across 12 patients with unique geometrical characteristics from the Bratislava dataset. The transfer matrices were computed using the boundary element method. Subsequently, these optimal electrode placements were used to compute the inverse solution for localizing the origin of premature ventricular contraction (PVC) with a single dipole cardiac source. The localization error (LE) was computed as the Euclidean distance between the true PVC origin, obtained through an invasive radiofrequency ablation, and the inverse solution. This enabled a direct comparison of LE computed for each optimal electrode placement with that from the full 128-electrode set.

**Results:** Results showed that subsets of electrodes, particularly 32 to 112, provided comparable localization accuracy (LE of  $30.5 \pm 15.0$  mm and  $26.8 \pm 12.6$  mm) to the full 128-electrode set (LE of  $27.2 \pm 11.5$  mm). High errors were observed with 8 and 16-electrode placements (LE of  $48.6 \pm 21.3$  mm and  $41.0 \pm 18.3$  mm).

**Conclusion:** Precise PVC localization can be achieved using strategically positioned subsets of electrodes, offering advantages in reduced preparation time, enhanced patient comfort, and improved cost-effectiveness of body surface potential mapping.

## 1. Introduction

Body surface potential mapping (BSPM) is the extension of the standard 12-lead ECG. During BSPM, tens of electrodes on the patient's torso are used to record the heart's electrical activity in the form of body surface potentials (BSPs) [1]. By using a larger number of electrodes during BSPM, more comprehensive and detailed information about the heart's electric field can be captured, surpassing the capabilities of a standard 12-lead ECG. The research showed that the BSPM could serve as a non-invasive diagnostic tool for various cardiac conditions [2,3] or for the response prediction of patients undergoing cardiac resynchronization therapy [4].

Several studies investigated the feasibility of using a reduced number of torso electrodes for BSPs recordings and interpreting them clinically for various diseases. These studies aimed to assess whether important information is preserved in recordings when using a subset of electrodes,

compared to the comprehensive mapping with numerous torso electrodes. The findings indicate that an optimal number of electrodes for this purpose is around 30 [5–7] with a minimum of 24 electrodes [8]. In every configuration, electrodes were primarily positioned on the front side of the torso, particularly in regions with high gradients. However, some electrodes were also positioned on the back. Despite these findings, the BSPM is not yet commonly employed as a standalone diagnostic tool in clinical practice.

However, BSPM holds significant importance in addressing the inverse problem of electrocardiography, which is highly relevant in clinical settings. The solution of the inverse problem of electrocardiography, i.e., Electrocardiographic Imaging (ECGI), refers to the estimation of electrical activity within the heart. This is achieved by using BSPs recorded using up to hundreds of electrodes positioned on the patient's chest and back [9,10], along with patient-specific geometrical models obtained from CT/MRI scans [11]. As a result, non-invasive estimation of electrical activity becomes possible, allowing for its identification in

\* Corresponding author. Institute of Measurement Science, Slovak Academy of Sciences, Dubravská cesta 9, 841 04, Bratislava, Slovakia.

E-mail address: [jana.svehlikova@savba.sk](mailto:jana.svehlikova@savba.sk) (J. Svehlikova).

## Abbreviations

BSPM	Body Surface Potential Mapping
BSPs	Body Surface Potentials
ECGI	Electrocardiographic Imaging
RFA	Radiofrequency Ablation
PVC	Premature Ventricular Contraction
NICD	National Institute of Cardiovascular Diseases
SVD	Singular Value Decomposition
RRE	Relative Residual Error
LE	Localization Error
LV	Left Ventricle
RV	Right Ventricle
RVOT	Right Ventricular Outflow Tract

the 3D model of the heart or “images,” facilitating a deeper understanding of activation spreading patterns through the heart [12,13]. It was shown that the solution of the inverse problem can be used to localize abnormal heart activity, such as identifying the origin of atrial [14] or ventricular arrhythmias [15]. Thus, the solution of the inverse problem can help to reduce the time and increase the success rate of radiofrequency ablation (RFA) procedures [16] or to guide non-invasive cardiac radio-ablations [17].

Regrettably, the use of numerous torso electrodes is one of the obstacles preventing the integration of the solution of the inverse problem into daily clinical practice. Using fewer torso electrodes would simplify the setup process, could enhance patient comfort during recording and improve the overall efficiency and cost-effectiveness of the method. After all, one could argue that due to the smooth character of the mapping from the electric heart activity to torso potentials, overly dense torso coverage is not needed when the inverse task is considered. Several studies investigated the quantity and spatial arrangements of electrodes required to address the inverse problem accurately. In the study by Gharbalchi No et al. [18], the sequential approach for the selection of torso electrodes was used, finding that 64 electrodes out of 192 produced accurate reconstructions of epicardial potentials by the solution of the inverse problem compared to 32 electrode setup. In the 64-electrode setup, the majority of electrodes were positioned anteriorly, with few located posteriorly. In the 32-electrode setup, all electrodes were situated anteriorly in the upper half of the torso. Parreira et al. [19] emphasized the importance of using an even larger number of electrodes (74) for improved spatial resolution, representing 33 % of the full set of electrodes. Cluitmans et al. [20] found stable reconstruction accuracy with 59 electrodes positioned anteriorly as well as posteriorly compared to the full set of 169 electrodes. The results of these studies do indeed support the intuition expressed above that a smaller set of electrodes may be sufficient when solving the inverse problem.

As outlined above, various studies explored optimal configurations of electrodes for solving the inverse problem, but results vary due to differences in BSPM systems (positions and number of electrodes) and inverse problem-solving approaches across research teams. Hence, this study aims to identify the optimal placements of electrodes for the solution of the inverse problem assuming a single dipole cardiac source with an aim to localize the origin of premature ventricular contractions (PVCs). The optimal electrode positions (out of 128 regularly placed electrodes on the torso) are determined through an analysis of the transfer matrix as a linear operator, focusing solely on the geometric and conductive properties of the torso. Additionally, the accuracy of the inverse solution in the localization of the origin of PVCs is explored using the proposed optimal electrode placements. Thus, we can investigate whether we can solve the inverse problem with a single dipole cardiac source accurately using a smaller number of electrodes on the patient’s torso.

## 2. Data and methods

### 2.1. Bratislava data

Twelve patients (9 males, 3 females; mean age  $54 \pm 17$  years) exhibiting spontaneous PVCs were used in this investigation. Data acquisition was conducted by the Institute of Measurement Science, Slovak Academy of Sciences, in collaboration with the National Institute of Cardiovascular Diseases (NICD) in Bratislava, Slovakia. Ethical approval was obtained from the Ethical Committee of NICD (ref. number F.050.2a, date of the decision March 17, 2020, issued March 19, 2020), and informed consent was obtained from participating patients. The study followed the principles of Good Clinical Practice and the Helsinki Declaration for Biomedical Research. More detailed information about the data acquisition and processing can be found in Refs. [21,22]. All patients who participated in the study underwent successful treatment of PVC by RFA procedure within the time range of 0 up to 425 days following the BSPM mapping. The details about the Bratislava dataset are summarized in Table 1.

#### 2.1.1. Signal processing

BSPs were recorded using the ProCardio 8 measuring system [23], which captures heart electrical activity through 128 evenly distributed torso electrodes integrated into self-adhesive strips (8 electrodes per strip). To maximize the number of captured PVCs, heart activity was recorded for 5–20 min at a sampling frequency of 1000 Hz. Signal preprocessing included the identification and elimination of broken leads [24] and the removal of the baseline drift using a high-pass filter (Blackmann-Harris window with 0.5 Hz cut-off frequency) [21]. R peaks in lead II of the standard 12-lead ECG were detected using the Pan-Tompkins algorithm [25]. Sinus beats and PVC beats were differentiated using the k-means clustering algorithm [26]. The individual numbers of PVC beats for each patient are summarized in Table 1. The average number of recorded PVC beats was  $219 \pm 170$ . These beats were averaged for each lead. The origin of the PVCs was manually identified, and the initial offset in the averaged PVC signals was removed by shifting the signal to zero [27]. Lastly, a BSP map  $\phi^{128 \times 30}$  was computed for each patient, representing the first 30 ms of the cardiac cycle. More detailed information about the signal processing can be found in Ref. [21].

#### 2.1.2. Geometrical modelling

After BSPM, CT scans of each patient were obtained using the Toshiba Aquilion One CT scan. These CT scans served as the basis for constructing geometrical models of the ventricles (endo-epicardium) and torso by the Tomocon software (<https://tatramed.sk/en/tomoco>)

**Table 1**

The information about the Bratislava dataset. The patient gender is denoted as M for male and F for female. The origin of premature ventricular contractions (PVC) is classified as originating from either the right ventricle (RV) or the left ventricle (LV).

Patient ID	Age [years]	Gender [M/F]	Time between BSPM and RFA [days]	PVC origin [RV/LV]	Number of beats [-]
P001	17	M	178	RV	62
P002	63	M	282	RV	9
P004	72	F	5	RV	210
P006	56	M	350	LV	39
P008	46	M	2	RV	267
P010	59	M	331	RV/LV	203
P021	33	M	61	LV	110
P023	38	M	384	RV	305
P024	79	M	8	LV	133
P027	57	F	425	RV	312
P029	64	F	0	RV	366
P036	61	M	157	LV	616

n-go/). Additionally, this software was used to capture the positions of torso electrodes. The resulting geometrical models were represented as 3D triangle geometrical meshes depicted in Fig. 1 for all patients.

### 2.1.3. Ground truth

Validating the accuracy of the inverse solution requires knowledge of the ground truth. Here, the ground truth position corresponds to the origin of the PVC determined during the RFA procedure. After the RFA procedure, ablation points were manually pinpointed on the ventricular mesh model by the cardiologist using procedure notes and data from intracardiac mapping systems. When multiple ablation points were present, the coordinates of the “representative ablation point” were calculated as the mean of these ablation points. The average distance from the “representative ablation point” to the ablation points, computed across all patients, was found to be 3.3 mm. The origin of PVC for each patient is shown in Table 1, where RV indicates the origin in the right ventricle and LV indicates the origin in the left ventricle.

## 2.2. Methods

The pipeline of this study is depicted in Fig. 2 and each part is described in more detail below.

### 2.2.1. Significance of the torso electrodes for a given dipole source position

In this work, the inverse problem is addressed using a single dipole cardiac source. Therefore, the objective of the inverse solution is to identify the position of the cardiac source, represented by a single dipole, that best characterizes the provided set of input data (torso potentials). The geometrical models of the torso and heart were used for the computation of the transfer matrix  $A$  by the boundary element method. In this context, the transfer matrix  $A$  represents the relationship between potentials observed at the torso surface and a cardiac source represented by a single dipole at a specific location. In the following computations, we assume a homogeneous torso model with isotropic conductivity properties.

It was shown that the significance of the torso electrodes for the solution of the inverse problem with a single dipole cardiac source depends on the origin of the cardiac activity [22]. The significance of each torso electrode was determined by analysing the singular values obtained from the singular value decomposition (SVD) of the transfer matrix  $A^{l \times 3}$  computed for a given dipole with 3 orthogonal components and  $l$  torso electrodes. In these calculations, the number of electrodes  $l$  ranged from 4 up to 128, incrementing by one in each step. The compact SVD of the transfer matrix  $A^{l \times 3}$  can be written as

$$A = U\Sigma V^T, \quad (1)$$

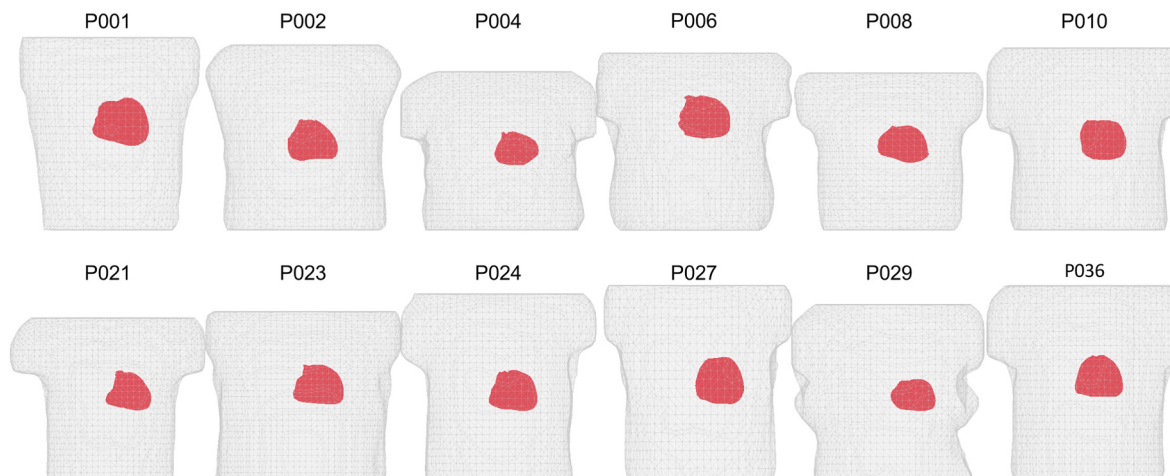


**Fig. 1.** The geometrical models of the torso (grey) and heart ventricles (pink) for each patient of the Bratislava data.

where  $U^{l \times 3}$ ,  $V^{3 \times 3}$  and  $\Sigma^{3 \times 3}$ . It applies that  $l > 3$  and thus the matrix  $\Sigma$  can have maximally 3 non-zero singular values sorted as  $\sigma_1 \geq \sigma_2 \geq \sigma_3$ . Loosely speaking, these singular values quantify how much of a signal at a particular dipole position is transferred to various torso electrodes via the linear operator  $A$ . In this work, we were looking for combinations of electrodes that maximized the total variation computed as the sum of all three singular values. The sum of singular values represents the trace norm of the operator  $A$  and can be viewed as a continuous generalization of the notion of the operator rank. One could select also other criteria to estimate the significance of torso electrodes such as product of singular values or the conditioning number. The product of singular values reflects the scaled volume of the transformation, while the condition number measures how sensitive a transfer matrix is to changes. In our study, the transfer matrices for individual cardiac dipole sources were generally well-conditioned, with an average condition number of  $1.6 \pm 0.6$  across all dipoles, lead placements, and patients. Because of this well conditioning, we chose the sum of singular values as a suitable criterion for our analysis. We have previously tested all these three criteria in detail [28].

Testing all possible combinations of electrodes meeting this criterion is computationally infeasible, so a greedy selection of torso electrodes was implemented. This involves selecting the best initial combination of four electrodes from all possible combinations ( $C(128, 4) = 10,668,000$ ) and then iteratively adding one electrode at a time to satisfy the criteria of maximized sum of singular values as best as possible. The greedy electrode order, where electrodes were sorted in descending order of significance, was determined for a given dipole. More details about the method and the greedy selection can be found in Ref. [22].

### 2.2.2. Significance of the torso electrodes regardless of dipole source position

Using this approach, the significance of torso electrodes is estimated for a given position of a dipole, representing the equivalent cardiac source. Nevertheless, one would like to determine which electrodes on the torso are the most significant for the solution of the inverse problem irrespective of the cardiac source's position and the geometrical properties of the patient. Therefore, we are interested in the “universally optimal” electrode placement that could be used across all patients.

To determine optimal electrode placement, the significance of the torso electrodes was computed for all possible positions of dipoles corresponding to all nodes of the 3D ventricular meshes of all patients. To speed up the computations, higher density meshes ( $3726 \pm 772$  nodes) were transformed into lower density ( $550 \pm 1$  nodes), regularly spaced meshes using software MeshLab (<https://www.meshlab.net/>) and

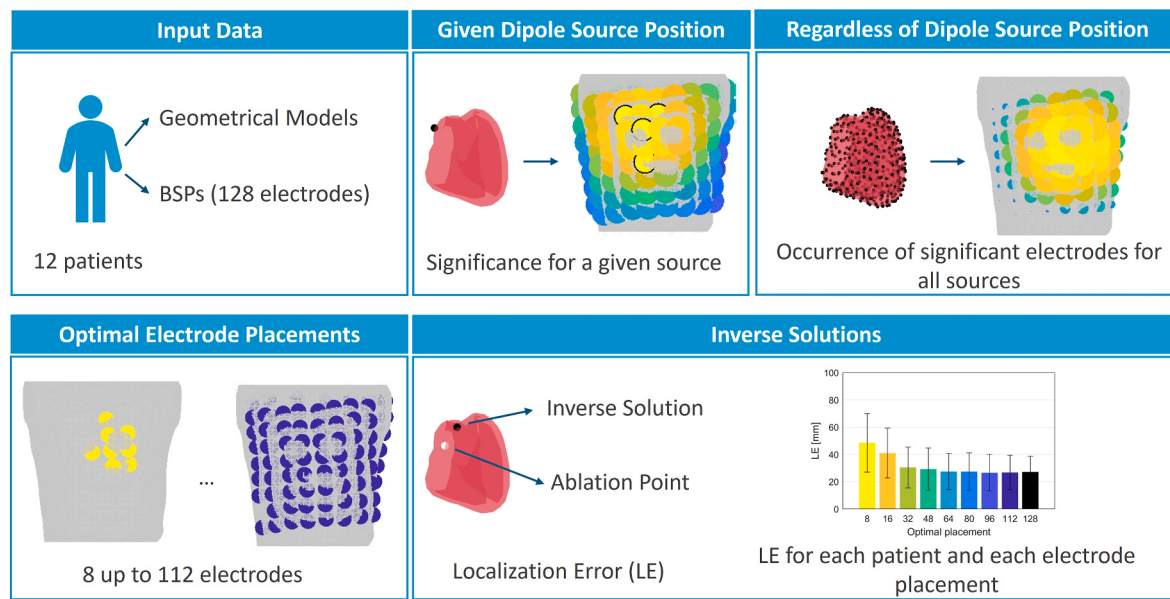


**Fig. 2.** The pipeline of this study.

iso2Mesh Matlab toolbox (<https://iso2mesh.sourceforge.net/cgi-bin/index.cgi>). The average distance between nodes was  $8.93 \pm 0.80$  mm. This assessment of torso electrode significance was performed for all patients and all dipole positions, thereby accounting for the geometric variations between individual patients.

#### 2.2.3. Optimal electrode placements

The optimal electrode placement was derived from all greedy orders of electrodes in which the electrodes are sorted from the most to the least significant. With an assumption of  $550 \pm 1$  dipoles and 12 patients, the total number of generated greedy orders was 6594. For each dipole source and each patient, the 32 most significant electrodes were selected, representing 25 % of the total set of 128 electrodes. These 32 electrodes selected for all studied patients contained 112 of the original set of 128 electrodes. Finally, the optimal placements of 8, 16, 32, 48, 64, 80, 96 and 112 electrodes were identified as the electrodes that occurred most frequently among these 32 patient-specific highly significant electrodes.

#### 2.2.4. Inverse solutions

When establishing the optimal electrode placements, the next objective was to examine the accuracy of the solution of the inverse problem using these reduced sets of electrodes. The inverse problem was solved for each position of the cardiac source  $S$  described as a single dipole using the equation

$$S = A^{+l} \Phi, \quad (2)$$

where  $A^{+l \times 3}$  is a pseudoinverse of the transfer matrix  $A$ ,  $\Phi^{l \times 30}$  is a potential map and  $l$  is the number of torso electrodes. The solution focuses on the first 30 ms of the cardiac cycle. This choice is based on the assumption that the activated region during this time span is small enough to be effectively represented by a single dipole [29]. The best representation of the electrical activity was determined by selecting the cardiac source  $S$  that resulted in the lowest relative residual error (RRE) computed between the measured map  $\Phi$  and the inversely estimated map using the Euclidean norm. The inverse problem was solved using derived optimal placements and thus the number of electrodes  $l$  ranged from 8 up to 112 electrodes. Finally, the inverse problem was solved using the full set of electrodes ( $l = 128$ ). The inverse problem was solved for all patients assuming a homogeneous torso model. More details about the inverse solution with a single dipole cardiac source can be

found in Refs. [12,21].

The accuracy of the inverse solution was assessed using the localization error (LE), quantifying the Euclidean distance between the position of the ground truth (ablation point) and the inverse solution (dipole position).

## 3. Results

The significance of the torso electrodes was computed for each possible position of the cardiac source defined by the triangular mesh of the heart model. Fig. 3 shows the greedy order of electrodes for patient P001 for the cardiac source placed in the base of the right ventricle (RV), the apex of the left ventricle (LV) and the base of the LV. The significance of electrodes is unitless, as it simply represents the order of electrodes sorted based on the criterion of maximizing the sum of singular values. Consequently, there are no units in the following figures, and the range is from 1 to 128 (full set of electrodes). The most significant electrode is depicted in bright yellow, while the least significant is shown in dark blue colour. These 3 cardiac sources exhibited a high distance between each other. For example, the distance between the cardiac source in the base of the RV and the source in the apex of the LV was 118.1 mm. From Fig. 3 it is evident that the positions of the most significant electrodes vary depending on the location of the cardiac source.

The greedy orders of electrodes were computed for all cardiac sources evenly placed on the ventricular mesh. Fig. 4 shows which electrodes occurred most frequently among the 32 most significant ones for patients P001, P029 and all patients considering all cardiac sources. The patients P001 and P029 were selected for illustrative purposes due to their distinct geometrical properties. In the bar graphs (panel A), each electrode is depicted as a bar, with its height indicating its frequency of occurrence. The exact positions of the electrodes and their occurrences are also depicted on the torso (panel B), where the size and colour of the electrode correspond to its occurrence. It is evident that certain electrodes appeared frequently among the top 32, while others were not identified at all. For example, the 36th electrode occurred among the 32 most significant ones for all considered cardiac sources (550) for patient P001 and thus its occurrence is 100 %. In patient P001, 6 electrodes occurred among the most significant ones for more than 90 % of dipoles (495 out of 550). In contrast, 25 out of 128 electrodes were not found among the 32 most significant ones. For patient P029, 5 electrodes occurred among the most significant ones for more than 90 % of dipoles

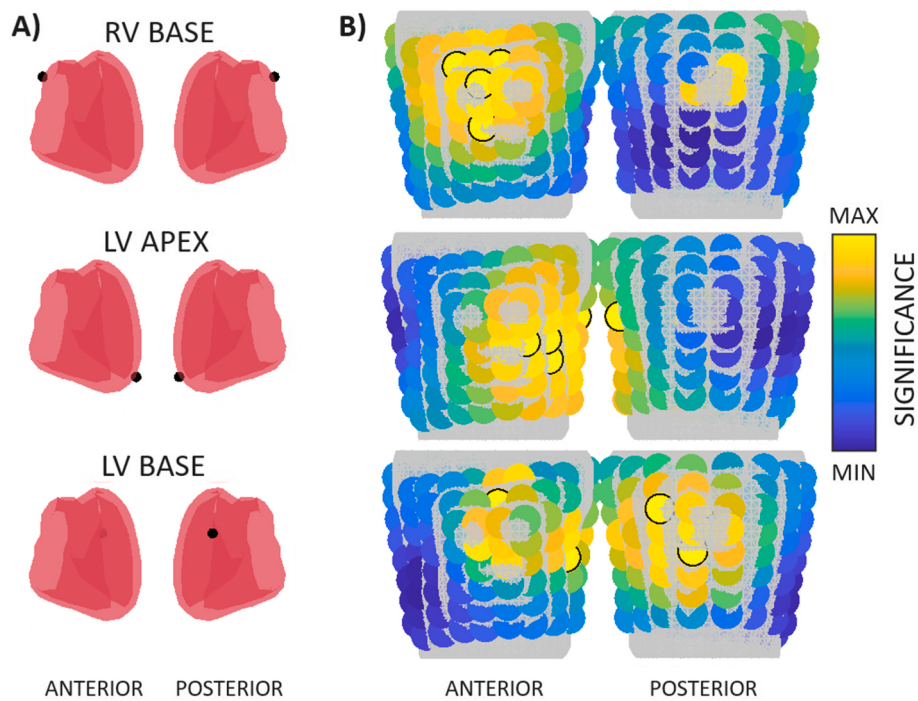


**Fig. 3.** A) The positions of the cardiac sources (black dots) located at the base of the right ventricle (RV), as well as the apex and base of the left ventricle (LV). The ventricles are depicted in their physiological positions within the torso. B) The greedy order of electrodes for the cardiac sources in panel A. The initial four electrodes are delineated by black circles, electrodes of maximum significance are indicated in yellow, while those of minimum significance are represented in the blue spectrum of colours. The colorbar on the right side corresponds to all 3 torsos. The anterior and posterior views are depicted.

and 48 electrodes were not identified among the most significant ones at all. Considering all patients, all electrodes appeared among the top 32 significant ones for all cardiac sources and 4 electrodes occurred among the most significant ones for more than 90 % of dipoles (5935 out of 6594). The lowest values of occurrence of some electrodes are close to zero and therefore cannot be seen in the corresponding plot. The placements of the electrodes on the torso that occurred most frequently are similar for patients P001, P029 and all patients. The most occurring electrodes for all dipole sources are placed anteriorly around the sternum and along the left sagittal plane, close to the heart's location. Additionally, some electrodes with a higher occurrence are also found posteriorly in the same region.

Based on the frequency of occurrences, the optimal electrode placements were derived as depicted in Fig. 5. For example, the 8-electrode optimal placement consists of 8 electrodes with the highest occurrence depicted in Fig. 4 for all patients. Given the positions of electrodes, the 8-electrode and 16-electrode placements consist of only anterior electrodes. The electrodes on the posterior side of the torso are selected from 32-electrode placement. The 112-electrode placement covers the whole torso except for the electrodes in the right posterior axillary line.

Next, the inverse problem was solved using the optimal electrode placements depicted in Fig. 5 and using a full set of 128 electrodes for all patients. Fig. 6 depicts the RRE maps across all patients and all electrode placements. The areas in red denote regions with the lowest RRE, indicating the segments that generate ECGs most similar to the recorded ECG. In contrast, areas in blue represent regions with the highest RRE. The origin of the PVC is found in the area of lowest RRE and the node with minimal RRE is depicted as white dot. Ablation points are represented by black dots. The minimal RRE value corresponding to the inversely computed origin of the PVC is presented in Table 2 for each patient and each optimal lead placement. The mean minimal RRE value across all patients and cases was  $0.16 \pm 0.06$ . Furthermore, cases where the inverse solution was located within the same ventricle as the ground truth were identified. These cases are indicated by stars, where a blue

star represents an inverse solution found in the correct ventricle with a LE of less than 25 mm while a red star denotes an inverse solution found in the correct ventricle with an LE exceeding 25 mm. Overall, the accuracy rate with respect to the ground truth position in the ventricles was 89 % for applicable cases.

The summary of results in terms of LE is shown in Fig. 7. Fig. 7 (panel A) and Table 3 show the LE values for each patient and each optimal electrode placement. It is evident that in almost all patients, the 8-electrode and 16-electrode placements resulted in high LE, whereas using a greater number of electrodes led to LE values similar to those observed when using all electrodes. This can be also seen in Fig. 7 (panel B) where the mean LE is depicted for each electrode placement. When using 8 and 16-electrode placements, higher LE was observed, with values of  $48.6 \pm 21.3$  mm and  $41.0 \pm 18.3$  mm across all patients, compared to an LE of  $27.2 \pm 11.5$  mm obtained using all 128 electrodes. However, better results were achieved using 32 and 48-electrode placements, with LE values of  $30.5 \pm 15.0$  mm and  $29.3 \pm 15.4$  mm, respectively. Interestingly, similar levels of accuracy to using the full set of electrodes were observed for 64 and 80-electrode placements, yielding LE values of  $27.5 \pm 13.2$  mm and  $27.5 \pm 13.6$  mm, respectively. Moreover, 96 and 112-electrode placements produced LE values of  $26.6 \pm 13.4$  mm and  $26.8 \pm 12.6$  mm, slightly surpassing the performance of all electrodes. Lastly, Fig. 7 (panel C) shows the distribution of LE values for a given patient using 8 up to 128 electrode placements. Therefore, each box represents the statistical distribution of 9 values. Similarly, the outliers correspond to the LE values obtained using electrode placements with a small number of electrodes. It transpires that in certain patients, the LE exhibited more variability using different numbers of electrodes as observed e.g., in patients P002, P006 and P023. In contrast, the LE remained quite similar across different electrode placements for some patients, as observed e.g., in patients P001, P008, and P010.

#### 4. Discussion

In this work, we proposed a method to estimate the significance of

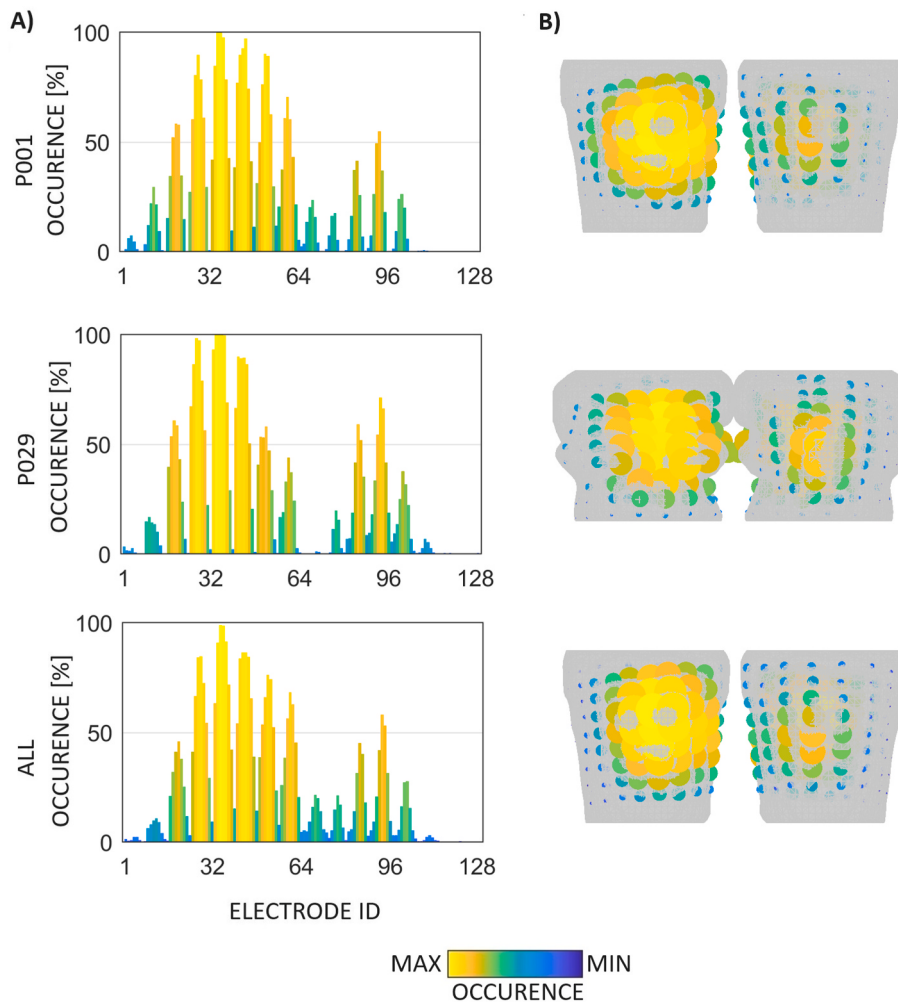


**Fig. 4.** The occurrence of each electrode among the 32 most significant electrodes computed for all dipoles, analysed separately for patients P001 and P029, as well as collectively for all 12 patients. The occurrence is represented by colour where the most occurring electrodes are depicted in yellow and the least occurring in blue colour spectra. A) The occurrence depicted in bar plots. B) The occurrence of electrodes depicted on the torso. Here, the occurrence is represented by the colour as well as by the size of the electrode. The anterior and posterior views are depicted.

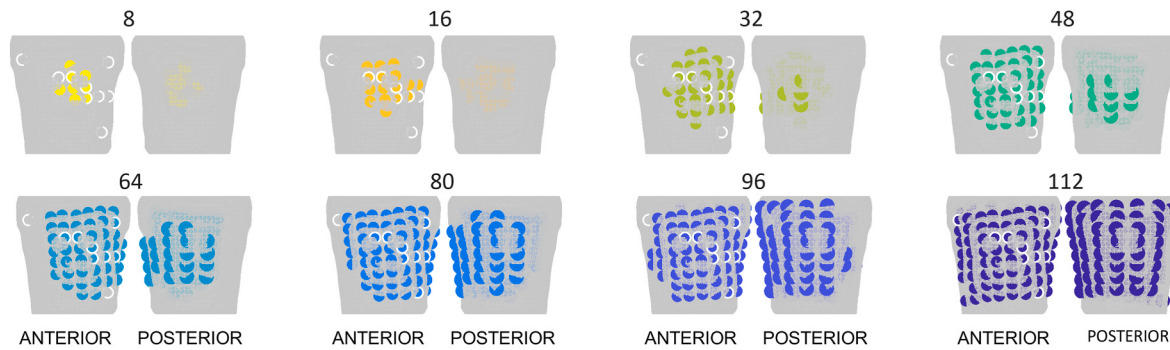


**Fig. 5.** Optimal placements of 8, 16, 32, 48, 64, 80, 96 and 112 electrodes depicted using geometry of patient P001. The approximate positions of the standard 12-lead ECG electrodes are shown within the white frame.

the torso electrodes irrespective of the cardiac source position and thus the optimal placement of electrodes could be derived. The significance of the electrodes was determined based on the transfer matrix, which considers only the geometric and electrical properties of the volume conductor. Fig. 3 shows that the positions of the most significant electrodes are in the relationship with the position of the cardiac source as we also showed in Ref. [22]. For instance, the apex of the ventricles is

positioned anatomically closer to the anterior side of the torso, slightly to the left of the sternum and near the diaphragm. This region is where the most significant electrodes were placed when estimating for cardiac source located in the apex of the ventricles. The base of the RV is anatomically situated more towards the anterior upper side of the torso, close to the sternum and this area is where significant electrodes were located when estimated for cardiac source in the base of RV.

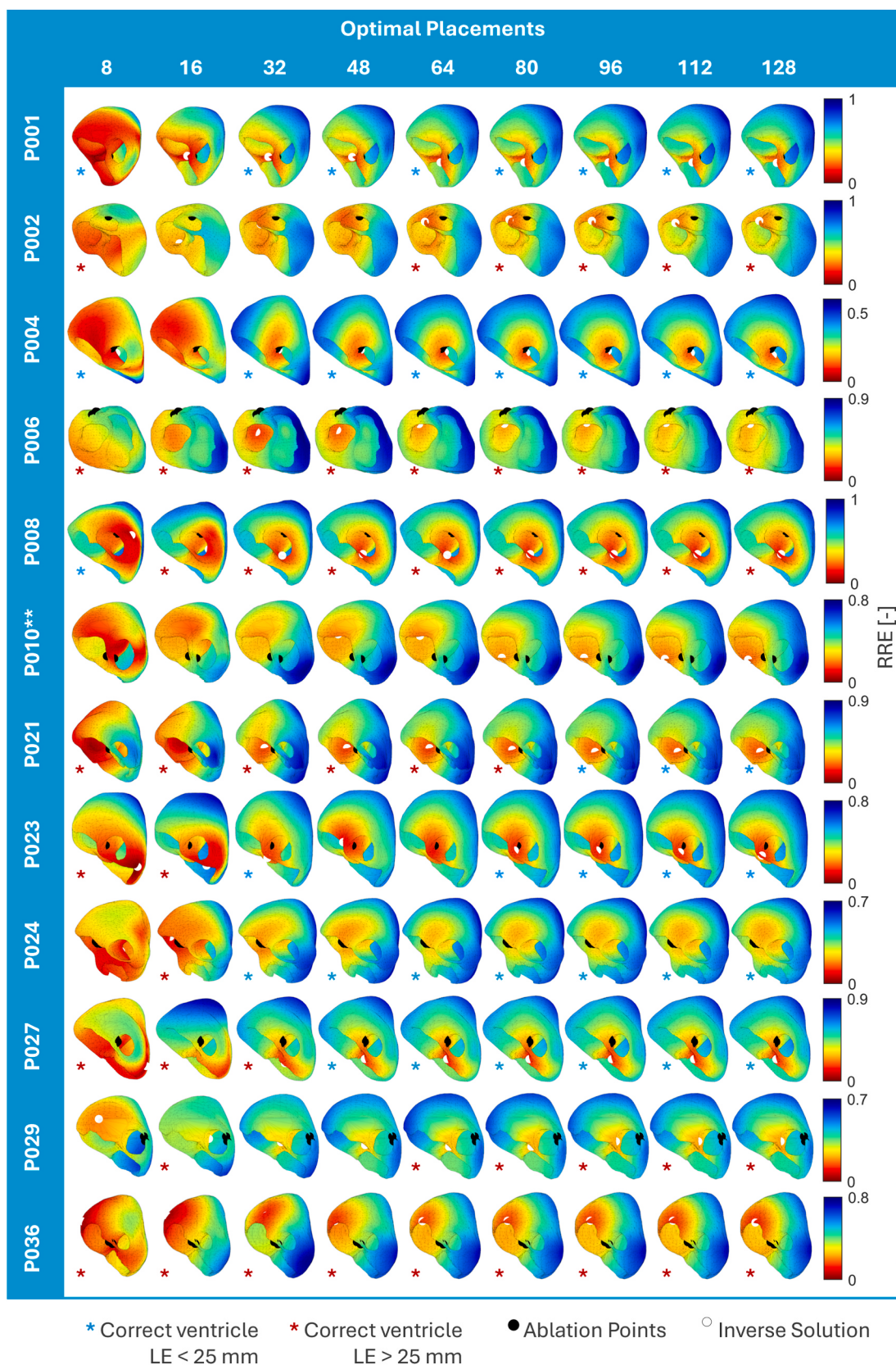


**Fig. 6.** Distribution of relative residual error (RRE) depicted on the ventricular geometry for each patient and lead placement. The ventricles are depicted from various angles for each patient to visualize specific areas of interest. Low RRE values are depicted in red, while high RRE values are shown in blue. Ablation points are indicated by black dots, and the position of the inverse solution (the node with minimal RRE) is marked by a white dot. Cases where the inverse solution was found in the same ventricle as the ablation site are indicated by stars. A blue star represents cases where the inverse solution was found in the correct ventricle with a localization error (LE) of less than 25 mm, whereas a red star indicates cases where the inverse solution was found in the correct ventricle but with an LE exceeding 25 mm. The ablation sites for P010\*\* were found in both ventricles, making it impossible to apply this analysis to that patient.

**Table 2**

The minimal RRE values corresponding to the inversely estimated origin of the PVC obtained for each patient and each electrode placement.

Patient ID	Optimal electrode placement								
	8	16	32	48	64	80	96	112	128
P001	0.00	0.11	0.17	0.20	0.18	0.20	0.20	0.20	0.20
P002	0.11	0.30	0.23	0.21	0.21	0.22	0.22	0.25	0.25
P004	0.02	0.06	0.10	0.11	0.11	0.11	0.12	0.12	0.12
P006	0.23	0.21	0.17	0.20	0.24	0.26	0.25	0.28	0.28
P008	0.06	0.10	0.15	0.16	0.15	0.16	0.15	0.15	0.15
P010	0.04	0.14	0.19	0.19	0.19	0.22	0.21	0.19	0.18
P021	0.01	0.06	0.19	0.18	0.18	0.19	0.20	0.20	0.19
P023	0.01	0.07	0.14	0.11	0.13	0.13	0.13	0.14	0.13
P024	0.08	0.10	0.15	0.15	0.19	0.19	0.18	0.17	0.17
P027	0.04	0.10	0.15	0.16	0.14	0.15	0.15	0.15	0.15
P029	0.18	0.26	0.21	0.23	0.22	0.22	0.21	0.21	0.21
P036	0.04	0.04	0.12	0.13	0.15	0.15	0.14	0.14	0.13

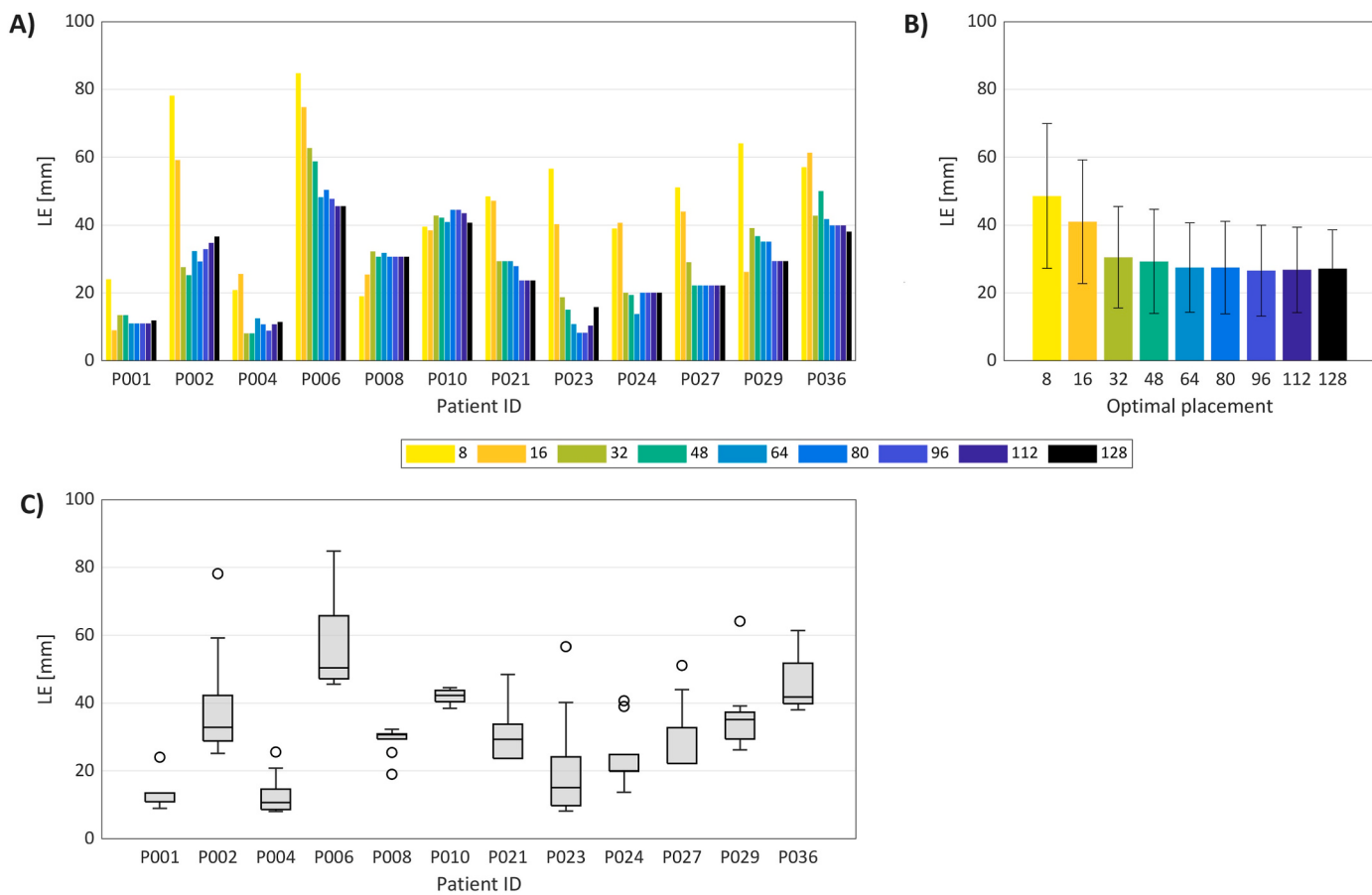


**Fig. 7.** A) The values of LE in mm obtained for each patient and each electrode placement. B) The mean LE values in mm and their standard deviations for each electrode placement. C) The boxplot of LE values obtained using 8 up to 128 electrode placements for a given patient.

Anatomically, the cardiac source placed in the base of the LV is placed closer to the posterior torso. Interestingly, the most significant electrodes were localized anteriorly and posteriorly for the cardiac source placed in the base of the LV ventricle.

Nevertheless, some electrodes on the torso will occur among the most significant ones for almost all possible positions of cardiac source as can be seen in Fig. 4. The positions of electrodes that occurred most frequently among the 32 most significant ones for all dipoles and all patients are similar to results that were observed for the rest of the patients and thus for illustrative purposes patients P001 and P029 were selected. In all three cases (P001, P029 and all patients), the majority of the most significant electrodes are placed anteriorly on the left side of the sternum, and some are placed posteriorly on the left side of the spine.

The prevalence of anterior electrodes can be explained by relationship between Figs. 3 and 4. The significant electrodes corresponding to cardiac sources situated nearer to the anterior torso are predominantly positioned anteriorly, while those associated with sources closer to the posterior torso are distributed on both sides of the torso. Thus, regardless of the positioning of cardiac sources, the majority of electrodes are anticipated to be situated on the anterior side of the torso.

The optimal placements of electrodes, regardless of the positioning of cardiac sources, were determined by identifying the most frequently occurring electrodes among the most significant ones across all patients and cardiac sources. These optimal placements are illustrated in Fig. 5. In all cases, the previous placement serves as a subset of the current placement; for example, the 8 electrodes used in the 8-electrode

**Table 3**

The values of LE in mm obtained for each patient and each electrode placement.

Patient ID	Optimal electrode placement								
	8	16	32	48	64	80	96	112	128
P001	24.0	9.0	13.4	13.4	11.0	11.0	11.0	11.0	11.9
P002	78.2	59.2	27.6	25.2	32.3	29.3	32.9	34.8	36.6
P004	20.9	25.6	8.1	8.1	12.5	10.7	8.9	10.7	11.4
P006	84.8	74.8	62.7	58.8	48.2	50.4	47.7	45.6	45.6
P008	19.0	25.4	32.3	30.7	31.8	30.7	30.7	30.7	30.7
P010	39.5	38.5	42.8	42.2	40.9	44.5	44.5	43.5	40.7
P021	48.5	47.2	29.4	29.4	29.4	27.9	23.7	23.7	23.7
P023	56.7	40.2	18.7	15.0	10.8	8.2	8.2	10.3	15.8
P024	39.0	40.7	20.0	19.4	13.7	20.0	20.0	20.0	20.0
P027	51.1	44.0	29.1	22.2	22.2	22.2	22.2	22.2	22.2
P029	64.1	26.2	39.1	36.8	35.1	35.1	29.4	29.4	29.4
P036	57.1	61.4	42.8	50.1	41.8	39.9	39.9	39.9	38.1

placement are a subset of the 16 electrodes used in the 16-electrode placement. The optimal placements of 8 and 16 electrodes reveal that these electrodes are exclusively situated anteriorly around the spine and the left lateral side of the anterior torso. In the case of the 32-electrode placement, there are an additional 4 electrodes on the posterior torso, while for the 48-electrode placement, this number increases to 9 electrodes. The inclusion of posterior electrodes in the optimal electrode placement increases with the total number of considered electrodes. Furthermore, Fig. 5 illustrates that the electrodes situated on the right side of the posterior torso, in proximity to the right arm, are identified as the least significant. Unfortunately, comparing our optimal electrode positions with those from other studies is challenging due to the lack of explicit positions for torso electrodes. Nevertheless, in all studies, it was shown that the area on the torso close to the heart location should be covered more densely and this was shown for the BSPM for diagnostic purposes [5–7] and the BSPM for the solution of the inverse problem [18]. For instance, our results and results in Ref. [18] diverged mainly in the placement of 32 electrodes. The 32-electrode placement in Ref. [18] consists of only anterior electrodes while the placement depicted in Fig. 5 includes also posterior electrodes.

Then, the inverse problem was solved using the derived optimal placements of electrodes for all patients. Fig. 6 illustrates the distribution of RRE values on ventricular geometry. The RRE map offers insights into the LE. For instance, in patient P001 with 128-electrode placement, the area with low RRE is near the ground truth, indicating a small LE. In contrast, for patient P036 with the same electrode placement, the area with low RRE values is located in the LV free wall, far from the ground truth in right ventricular outflow tract (RVOT), indicating a high LE. The minimal RRE values are summarized in Table 2. The minimal RRE values showed small variability, with a standard deviation of 0.06. The highest minimal RRE value was 0.3, observed in patient P002 with the 16-electrode placement, which corresponded to a high LE value of 59.2 mm. However, this association was not consistent across all cases. For example, patient P036 with full electrode placement exhibited a relatively low minimal RRE value of 0.13, despite a higher LE value of 38.1 mm. The Pearson's correlation coefficient between the minimal RRE and LE values was 0.09, suggesting no or very weak positive correlation. Further, we investigated whether the inverse solution correctly identified the ventricle of origin. Overall, the accuracy rate was 89 %, with 38 % having an LE smaller than 25 mm and 51 % having an LE greater than 25 mm. Correct identification of the ventricle was also observed with 8-electrode and 16-electrode placements (8 out of 12 patients), although LE was higher in these cases. Interestingly, RRE maps for 8 and 16-electrode placements produce large areas with low RRE, complicating the identification of the node with the minimal RRE value. However, increasing the number of electrodes reduces the area with low RRE, making it easier to identify the node with the smallest RRE.

The results in terms of LE are summarized in Fig. 7 and Table 3. The results demonstrated that low accuracy in PVC localization was obtained

with 8-electrode and 16-electrode placements. In both cases, the mean LE exceeded 40 mm, and a higher deviation of LE values was observed among 12 patients. In contrast, several studies have shown that good localization by non-invasive mapping can be achieved using the standard 12-lead ECG [30,31]. However, this was not observed in our study, where high localization errors persisted even with 16-electrode placement, despite the correct identification of the ventricle. Our 16-electrode placement includes electrodes V1-V6, as shown in Fig. 5, but lacks the limb leads. Moreover, the 12-lead ECG configuration in Ref. [28] was adapted to include two additional electrodes on the patient's back. It is worth hypothesizing that including limb leads and some posterior electrodes might improve the accuracy of our solutions, a possibility that could be explored in future research. Interestingly, the mean localization accuracy improved to 30.5 mm using the 32-electrode placement, which is only 3.3 mm higher than when using the full set of 128 electrodes. This improvement can be attributed to the inclusion of posterior electrodes in the 32-electrode placement. With each added electrode, the localization slightly improved and with 96-electrode and 112-electrode placement it was even better than using a full set of electrodes. In these cases, 0.6 mm and 0.4 mm improvement were observed compared to using the full set, respectively. These findings indicate that the electrodes located along the right posterior axillary line are indeed insignificant and could contribute to errors in the solution.

The results demonstrate that for certain patients, achieving accurate solutions of the inverse problem does not require full torso coverage by electrodes. This is evident in Fig. 7, panel A. The subsequent discussion specifically addresses the outcomes associated with electrode placements of 32 and higher, as the findings suggest that the use of 8 and 16 electrodes led to high LEs. Improvements in localization accuracy compared to the full electrode set were observed for patients P001, P002, P004, and P023. In certain cases, the same accuracy was achieved using a subset of significant electrodes, as evidenced by patients P008, P024, and P027. However, regrettably, deterioration in PVC localization accuracy was observed in some patients such as P010 and P036. Nonetheless, the most significant deterioration of 17.1 mm compared to the full set was observed in patient P006. The LE using a full set of electrodes was very high for this patient (LE of 45.6 mm) and thus the results of the inverse solution for this patient may not be very reliable even with the full set of electrodes.

The results of this study suggest that the accurate localization of PVC origin can be obtained using a smaller set of electrodes. The results underscore the previous findings obtained using different methods [18–20]. In terms of inverse solution accuracy, patient preparation time, and patient comfort, the use of 64-electrode or 80-electrode placements demonstrates promising outcomes. However, if the patient has sensitive skin or could experience discomfort during measurement, employing the 32-electrode placement could be considered. Nonetheless, in such instances, a slight deterioration in localization accuracy may be anticipated.

This study has several limitations. Firstly, the optimal electrode placements were determined based on the properties of the transfer matrix derived from patient-specific geometrical models. However, accurately segmenting organs from CT/MRI scans poses challenges, and errors arising from segmentation may impact the analysis [32]. Additionally, the study was conducted using patient-specific models of only 12 patients, limiting its ability to encompass the diverse anatomical properties among individuals. The simplifications of complex biophysical properties (single dipole cardiac source, homogeneous torso model) were made to identify the optimal electrode placements and consequently to solve the inverse problem. Thus, those simplifications may impact the outcomes of this study. Furthermore, the optimal electrode placements were solely used to identify the origin of PVC, thus limiting the applicability of the results to other cardiac abnormalities. Additionally, the position of ablation points was marked by the cardiologist on the ventricular mesh after a successful RFA procedure, potentially leading to minor misplacements in terms of millimetres. Despite these limitations, the study highlights that accurate localization of PVC origin by the solution of the inverse problem with a single dipole cardiac source can be achieved using a smaller set of optimally placed electrodes.

## 5. Conclusion

This study determined the optimal placements of 8, 16, 32, 48, 64, 80, 96 and 112 electrodes by analysing the singular values of the transfer matrix. These optimal electrode placements were identified without regard to the position of the cardiac source and while taking into account various geometrical properties among patients. Identified electrode placements were used to compute the inverse solutions using a single dipole cardiac source with the objective of localizing the origin of PVC. The results demonstrate that 8 and 16-electrode placements show deteriorated performance compared to using the full set of 128 electrodes. However, when using 32-electrode placement, the average LE from 12 patients was only 3.3 mm higher than when using the full set. Interestingly, with a 64-electrode placement, the average LE was only 0.3 mm higher compared to the full set. Therefore, the study results emphasize the feasibility of using a reduced number of torso electrodes for an accurate solution of the inverse problem with a single dipole cardiac source. This could potentially lead to a more patient-friendly and cost-effective BSPM setup for clinical practice.

## CRediT authorship contribution statement

**Beata Ondrusova:** Writing – original draft, Visualization, Methodology, Formal analysis, Conceptualization. **Peter Tino:** Writing – review & editing, Supervision, Conceptualization. **Jana Svehlikova:** Writing – review & editing, Supervision, Project administration, Funding acquisition, Data curation, Conceptualization.

## Data availability statement

The authors will provide the raw data supporting the conclusions of this article, with no unnecessary restrictions or reservations. For further information about the data, please contact [jana.svehlikova@savba.sk](mailto:jana.svehlikova@savba.sk). For further information about the methodology and scripts generated within this study, please contact [beata.ondrusova@savba.sk](mailto:beata.ondrusova@savba.sk).

## Funding

This work received support from the joint project of the Slovak Academy of Sciences, Slovakia (grant number 536057) and TÜBITAK, Turkey (grant number 120N200). Further, it was supported by the VEGA Grant Agency, Slovakia under grant number 2/0109/22.

## Declaration of competing interest

The authors declare that they have no known competing financial interests or personal relationships that could have appeared to influence the work reported in this paper.

## Acknowledgments

The authors extend sincere gratitude to Dr. Peter Hlivak, PhD., from the National Institute of Cardiovascular Diseases, Slovakia, for his contribution during data acquisition and labeling of the ablation points on the heart's mesh. Additionally, the authors wish to acknowledge Mr. Jan Zelinka from the Institute of Measurement Science, Slovak Academy of Sciences, Slovakia, for his contribution to data processing.

## References

- [1] J. Bergquist, L. Rupp, B. Zenger, J. Brundage, A. Busatto, R.S. MacLeod, Body surface potential mapping: contemporary applications and future perspectives, *Heart (Lond.)* 2 (4) (2021) 514–542, <https://doi.org/10.3390/hearts2040040>.
- [2] M. Kania, et al., High-resolution body surface potential mapping in exercise assessment of ischemic heart disease, *Ann. Biomed. Eng.* 47 (5) (May 2019) 1300, <https://doi.org/10.1007/S10439-019-02231-2>.
- [3] M. Kloosterman, et al., Body surface potential mapping detects early disease onset in plakophilin-2-pathogenic variant carriers, *EP Europace*, 25 (7) (Jul. 2023) 1–12, <https://doi.org/10.1093/EUROPACE/EUAD197>.
- [4] R.M. Gage, A.E. Curtin, K.V. Burns, S. Ghosh, J.M. Gillberg, A.J. Bank, Changes in electrical dyssynchrony by body surface mapping predict left ventricular remodeling in patients with cardiac resynchronization therapy, *Heart Rhythm* 14 (3) (Mar. 2017) 392–399, <https://doi.org/10.1016/j.hrthm.2016.11.019>.
- [5] R.L. Lux, C.R. Smith, R.F. Wyatt, J.A. Abildskov, Limited lead selection for estimation of body surface potential maps in electrocardiography, *IEEE Trans. Biomed. Eng.* BME-25 (3) (1978) 270–276, <https://doi.org/10.1109/TBME.1978.326332>.
- [6] O. Dossel, F. Schneider, M. Muller, Optimization of electrode positions for multichannel electrocardiography with respect to electrical imaging of the heart, in: Proceedings of the 20th Annual International Conference of the IEEE Engineering in Medicine and Biology Society, IEEE, Nov. 2002, pp. 71–74, <https://doi.org/10.1109/imb.1998.745825>.
- [7] D.D. Finlay, C.D. Nugent, M.P. Donnelly, R.L. Lux, P.J. McCullagh, N.D. Black, Selection of optimal recording sites for limited lead body surface potential mapping: a sequential selection based approach, *BMC Med. Inf. Decis. Making.* 6 (1) (Feb. 2006) 1–9, <https://doi.org/10.1186/1472-6947-6-9>.
- [8] R.C. Barr, M.S. Spach, G.S. Herman-Giddens, Selection of the number and positions of measuring locations for electrocardiography, *IEEE Trans. Biomed. Eng.* 18 (2) (1971) 125–138, <https://doi.org/10.1109/TBME.1971.4502813>.
- [9] J. Kadanec, J. Zelinka, G. Bukor, M. Tysler, ProCardio 8 {\textemdash} System for high resolution ECG mapping, in: 2017 11th International Conference on Measurement, IEEE, 2017, pp. 263–266, <https://doi.org/10.23919/measurement.2017.7983586>.
- [10] Medtronic, *CardioInsight Mapping Vest*, 2022. *Medtronic*.
- [11] A.J. Pullan, L.K. Cheng, M.L. Buist, 09 the inverse problem of electrocardiology, *Mathematically Modelling the Electrical Activity of the Heart*. (2005) 329–373, [https://doi.org/10.1142/9789812775153\\_0007](https://doi.org/10.1142/9789812775153_0007).
- [12] Y.S. Dogrusoz, et al., Comparison of dipole-based and potential-based ECGI methods for premature ventricular contraction beat localization with clinical data, *Front. Physiol.* 14 (Jun. 2023) 1197778, <https://doi.org/10.3389/FPHYS.2023.1197778/BIBTEX>.
- [13] J. Duchateau, et al., Performance and limitations of noninvasive cardiac activation mapping, *Heart Rhythm* 16 (3) (Mar. 2019) 435–442, <https://doi.org/10.1016/J.HRTHM.2018.10.010>.
- [14] S. Yamashita, D.A. Hooks, G. Cheniti, P. Jais, High-density contact and noninvasive mapping of focal atrial tachycardia: evidence of dual endocardial exits from an epicardial focus, *Pacing Clin. Electrophysiol.* 41 (6) (2018) 666–668, <https://doi.org/10.1111/pace.13278>.
- [15] E. Wissner, et al., Noninvasive epicardial and endocardial mapping of premature ventricular contractions, *Europace* 19 (5) (2017) 843–849, <https://doi.org/10.1093/europace/euw103>.
- [16] L. Parreira, et al., Successful ablation of premature ventricular contractions exclusively guided by epicardial and endocardial non-invasive mapping (ECGI) and confirmed by substrate mapping, *J. Electrocardiol.* 62 (Sep. 2020) 103–106, <https://doi.org/10.1016/j.jelectrocard.2020.07.003>.
- [17] C.G. Robinson, et al., Phase I/II trial of electrophysiology-guided noninvasive cardiac radioablation for ventricular tachycardia, *Circulation* 139 (3) (Jan. 2019) 313–321, <https://doi.org/10.1161/CIRCULATIONAHA.118.038261>.
- [18] F. Gharbalchi No, et al., Reduced leadset selection and performance evaluation in the inverse problem of electrocardiography for reconstructing the ventricularly paced electrograms, *J. Electrocardiol.* 60 (May 2020) 44–53, <https://doi.org/10.1016/j.jelectrocard.2020.02.017>.

- [19] L. Parreira, et al., Electrocardiographic imaging ({ECGI}): what is the minimal number of leads needed to obtain a good spatial resolution? *J. Electrocardiol.* 62 (Sep. 2020) 86–93, <https://doi.org/10.1016/j.jelectrocard.2020.07.004>.
- [20] M.J.M. Cluitmans, et al., In-vivo evaluation of reduced-lead-systems in noninvasive reconstruction and localization of cardiac electrical activity, *Comput. Cardiol.* 42 (Feb. 2015) 221–224, <https://doi.org/10.1109/CIC.2015.7408626> (2010).
- [21] J. Svehlikova, et al., The importance of ECG offset correction for premature ventricular contraction origin localization from clinical data, *Meas. Sci. Rev.* 22 (6) (2022) 202–208, <https://doi.org/10.2478/msr-2022-0031>.
- [22] B. Ondrusova, P. Tino, J. Svehlikova, A two-step inverse solution for a single dipole cardiac source, *Front. Physiol.* 14 (Sep. 2023) 1264690, <https://doi.org/10.3389/FPHYS.2023.1264690>.
- [23] J. Kadanec, J. Zelinka, G. Bukor, M. Tyšler, ProCardio 8 - system for high resolution ECG mapping, *Measurement.* (2017) 263–266, <https://doi.org/10.23919/MEASUREMENT.2017.7983586>.
- [24] Y. S. Dogrusoz et al., “The Effects of Interpolating Bad Leads on the Solution of the Inverse Electrocardiography Problem,” pp. 1–14.
- [25] J. Pan, W.J. Tompkins, A real-time QRS detection algorithm, *IEEE Trans. Biomed. Eng.* BME-32 (3) (1985) 230–236, <https://doi.org/10.1109/TBME.1985.325532>.
- [26] Christopher M. Bishop, *Pattern Recognition and Machine Learning*, first ed., Springer, New York, 2006 <https://doi.org/10.1007/978-0-387-45528-0>.
- [27] J. Svehlikova, et al., The importance of residual PVC offset correction for inverse localization of PVC origin using a single dipole, *J. Electrocardiol.* 69 (Nov. 2021) 82–83, <https://doi.org/10.1016/J.JELECTROCARD.2021.11.009>.
- [28] B. Ondrusova, P. Tino, J. Svehlikova, A two-step inverse solution for a single dipole cardiac source, *Front. Physiol.* 14 (Sep. 2023) 1264690, <https://doi.org/10.3389/FPHYS.2023.1264690>.
- [29] J. Svehlikova, M. Teplan, M. Tyšler, Geometrical constraint of sources in noninvasive localization of premature ventricular contractions, *J. Electrocardiol.* 51 (3) (2018) 370–377, <https://doi.org/10.1016/j.jelectrocard.2018.02.013>.
- [30] K. A. Sedova, P. M. Van Dam, M. Blahova, L. Necasova, and J. Kautzner, “Localization of the Ventricular Pacing Site from BSPM and Standard 12-lead ECG: a Comparison Study,” 123AD, doi: 10.1038/s41598-023-36768-z.
- [31] S. Pezzuto et al., “Reconstruction of Three-Dimensional Biventricular Activation Based on the 12-lead Electrocardiogram via Patient-specific Modelling”, doi: 10.1093/europace/euaa330.
- [32] J.D. Tate, et al., Segmentation uncertainty quantification in cardiac propagation models, in: Computing in Cardiology, IEEE Computer Society, 2022, <https://doi.org/10.22489/CINC.2022.419>.